Experimental Comparison of Three Electro-textile Interfaces for Textile UHF-RFID Tags on Clothes

Chengyang Luo, Ignacio Gil and Raúl Fernández-García

[a]*Department of Electronic Engineering, Universitat Politecnica de Catalunya, Carrer de Colom 1, Terrassa, 08222, Barcelona, Spain*

Abstract

Textile Ultra High Frequency (UHF, 865-868 MHz) Radio Frequency Identification (RFID) devices meet difficulties from connection of solid chips and textile antennas. In this work, three electro-textile interfaces integrated with the corresponding textile UHF-RFID antennas as the solutions are proposed and compared. The simulated and measured impedance curves of the corresponding antennas are all close and the radiation performance (realized gain) are designed to be near (about 1.4 dBi). According to the Friis formula, the simulated and measured read ranges of the interfaces with the corresponding antennas in air are obtained (all above 4.5 m). For reliability validation, mixed use feasibility tests are implemented and the results show the read ranges of each interface used on other two designs have tolerable read range decrease ($<$ 2 m but all above 3.41 m).In addition, the read ranges of the designs on body are all above 2.05 m. Due to the small sizes of the interfaces, stable performance on body and good reliability, the proposed interfaces solutions are proved feasible.

Keywords: Electro-textile, Interface, UHF-RFID, antenna, mix use, feed port, read range, on body.

1. Introduction

With Radio Frequency Identification (RFID) technology development, many commercial devices are applied in diverse scenarios [1][2][3] such as health-caring monitoring [4], goods tracking [5][6], classification, localization and stuff management [7]. Most of them are developed by welding integrated circuit (IC) chips on a hard or flexible Printed Circuit Board (PCB) [8] or

a chipless way [9][10]. The welding technique for connecting chips to RFID antennas on PCBs is proven and reliable. However, this popular technique is not suitable for most textile RFID devices on clothes due to the high temperature intolerance (< 200°C) of the common knit yarns and fabrics [11][12][13]. Even for some wearable polymeric materials such as Polyvinyl Chlorid (PVC) fiber, alginate fiber and carbon fiber, the chips on them face the problem of unstable fixation.

To avoid this connection problem, some works are exploring free welding methods such as fixing with glue [14], non-conducting yarns or copper plates [15] [18]. In a study [15], a passive UHF-RFID-based knitted wearable compression sensor is proposed for monitoring a baby breathing activity, for which a chip (Monza R6) is welded on a FR4 PCB. Then the board with the chip is inserted into a small pocket knitted in the middle region of the antenna top layer. In another work [14], a textile UHF-RFID antenna solution concentration sensor is proposed and the chip is fixed by sewing and glue, which is more flexible for wearable applications. However, many similar designs are foreseen to have difficulties such as chip pads rust due to textile washing and the detachment of the chip-welded board in textile devices.

In this paper, three electro-textile interfaces integrated with the corresponding textile UHF-RFID antennas (by sewing, snap buttons and inserting) are proposed and compared to provide chip-textile connection solutions. Related preparatory work before simulation such as the detailed embroidery method and interface impedance tests is implemented and presented. Based on the accurate impedance of three electro-textile interfaces obtained by the real tests, the simulation of the corresponding antennas is developed and the simulated results are compared with the measured results. Note that the textile UHF-RFID antennas are designed to keep the maximum realized gain values near for next performance comparison. Finally, related reliability validation tests including mixed use reliability and use on body are implemented. The proposed electro-textile interfaces have the potential to be applied into thicker clothes such as winter clothes (not too close to bodies) due to their small sizes and stable performance.

2. Design and Related Details

2.1. Structure of the Proposed Electro-textile Interfaces

The geometry and configuration of the three proposed electro-textile interfaces with the corresponding textile UHF-RFID antennas are shown

in Fig. 1. Considering the common problem about the difficulty of the chips and textile interconnection, the three interfaces (type1 to 3) are proposed and analyzed for the textile UHF-RFID antennas and the UHF-RFID chip (LXMS21ACNP-184, impedance: 19-i*284 ohm, wake-up power: -18 dBm)[16][17] on the small PCBs. The three connection ways as shown in Fig. 1 are by sewing, snap buttons and inserting, respectively. Note that, all the interfaces have different complex impedance (not 50 ohm) from that of the chip. In addition, despite of using the same chips for the three interfaces , they have different complex impedance as feed ports due to the different structures and connection methods. Therefore, the textile UHF-RFID antennas are designed based on the corresponding complex impedance. The PCBs dimensions of the type 1, 2 and 3 are 12.7*6.22*0.8 mm, 16.38*31.12*0.8 mm and 7.76*6.10*0.8 mm, respectively. Moreover, the hole diameters of the type 1 and type 2 are 2 mm and 9 mm, respectively.

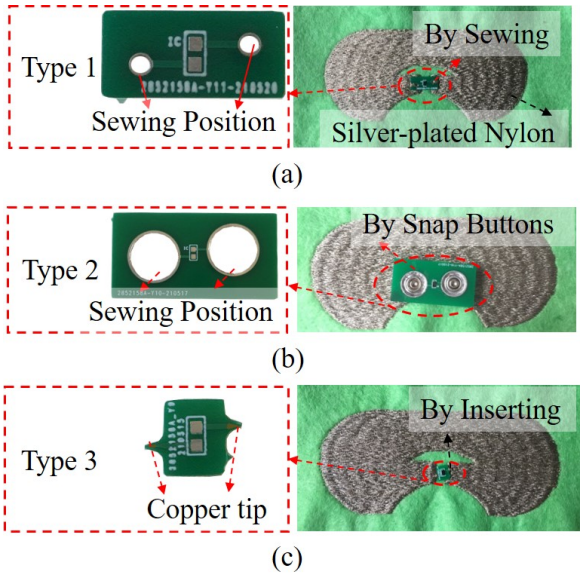

Figure 1: Geometry and configuration of the three proposed electro-textile interfaces with the corresponding UHF-RFID antennas. (a) Type 1, (b) Type 2, (c) Type 3.

The proposed textile UHF-RFID antennas are embroidered using conductive yarns as on a polyester fibers substrate. A commercial conductive twisted yarn made of 99% pure silver-plated Nylon is used as the textile material of the antenna, the bulk conductivity of which is 11500 siemens/m

with 0.2 mm thickness obtained by the previous works[14][15]. Moreover, the polyester is selected as the substrate, the relative dielectric constant, loss tangent and thickness of which are 1.29 (ε_r) 0.00188 (tanD) and 0.88 mm , respectively. In addition, the sewing yarns for the 'Type 1' are adopted the same as the conductive yarns of the antennas whereas the snap buttons for the 'Type 2' are made of steel.

2.2. Impedance Characterization

2.2.1. Impedance Measurement Method

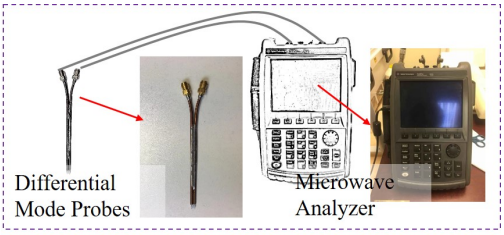

Figure 2: Calibration setup with the differential mode probes for impedance measurements method

For balanced structures, a popular method validated in some works[14] [19][20][21] for impedance measurements is to combine the function (port extension[22]) of the Microwave Analyzer (N9916A) with the differential mode probes as shown in Fig. 2. The probes are made from two semi-rigid cables with ground shields soldered together. Concerning to the procedure, first of all, the Microwave Analyzer with two coaxial cables needs to be calibrated by a standard calibration kit. Secondly, after connecting the coaxial cables to the differential mode probes, the function (port extension [22]) of the Microwave Analyzer needs to be adjusted in order to move the calibration plane from the ends of the coaxial cables to the ends of the differential mode probes. Meanwhile, the traces in Smith chart of the two ports should roughly converge to the open circuit position in the Microwave Analyzer. Next, the two tips of the differential mode probes are connected to the proposed textile UHF-RFID antennas or the feed port PCBs and the Z parameters in 50 ohms can be obtained. Note that the measured Z parameters using the differential mode probes are earth-referenced and need to be transferred for the differential reflection coefficient (ρ) of the balanced samples [23][24]. Finally, Z parameters of the tested samples in the complex conjugate impedance of the chip can be calculated using the equations 1 as follows,

$$Z_{ant} = \frac{2Z_0(1 - S_{11}S_{22} + S_{12}S_{21} - S_{12} - S_{21})}{(1 - S_{11})(1 - S_{22}) - S_{12}S_{21}} \quad (1)$$

Where Z_0 is 50 ohms, S_{11}, S_{12}, S_{21} and S_{22} are the measured S parameters, Z_{ant} is the Z parameter of the balanced samples.

2.2.2. Impedance Measurements of the Three Electro-textile Interfaces

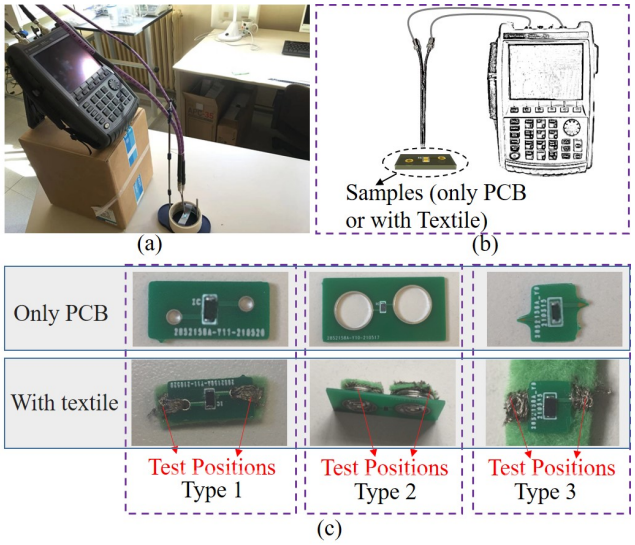

Figure 3: Experimental setup for the interfaces impedance. (a) Photograph of the setup, (b) Experimental setup configuration. (c) Tested cases ('Only PCB' and 'With Textile').

The impedance of the three interfaces is different when the chip is welded on the different PCBs and then connected to the textile materials. It is essential to obtain the accurate port impedance before designing antennas. The experimental setup for the complex impedance measurements is shown in Fig. 3 (a) and (b). As aforementioned, the differential measurement method with the differential mode probes is used. In addition, in order to reduce the impact from the connection, the interface impedance tests are conducted in the case of the three electro-textile interfaces ('With Textile') as shown in Fig. 3 (c).

After being calculated by equation 1, the measured impedance results of the three interfaces are shown in Fig. 4, including the resistance part and the reactance part. It is found that the resistance curves of the three types

has a difference of less than 5 ohm difference in the absolute value case while their reactance curves have obvious differences (about 20 to 60 ohm in the absolute value case). In addition, at 868 MHz, the complex impedance of the interfaces are listed in Table 1.

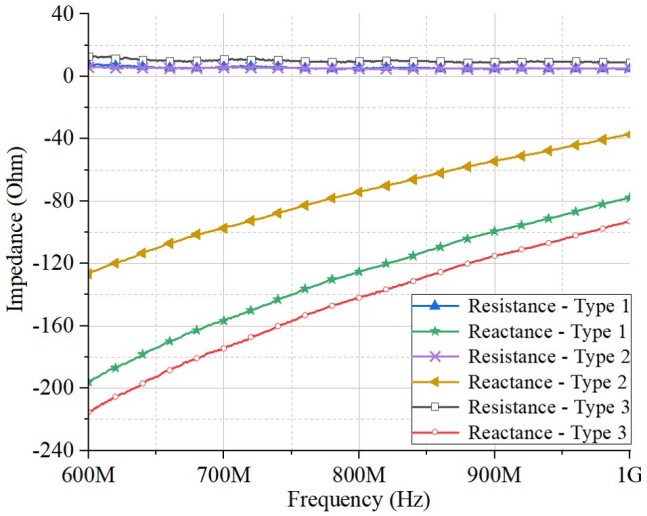

Figure 4: Measured impedance for the three electro-textile interfaces ('With Textile').

Table 1: Complex Impedance of the Interfaces at 868 MHz(Unit: Ohm)

Case	*Type* 1	*Type* 2	*Type* 3
With Textile	5.09-i*107.7	5.06-i*60.27	9.29-i*123.27

2.3. Simulation and Measurements

2.3.1. Simulation models of the corresponding textile antennas

After obtaining the measured complex impedance of the three electro-textile interfaces ('with textile'), the corresponding UHF-RFID antennas can be designed based on the measured impedance as feed port impedance. The fundamental model simulated in simulated in high-performance 3D EM analysis software (CST) is shown in Fig. 5 and the three corresponding textile antennas are developed by adjusting related dimension parameters based on the shown model. The dimension parameters of the three designed antennas are listed in the Table 2.

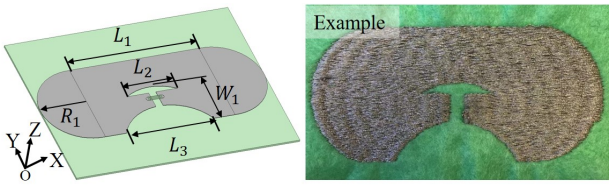

Figure 5: Geometry of the fundamental simulated model for the three corresponding UHF-RFID antennas.

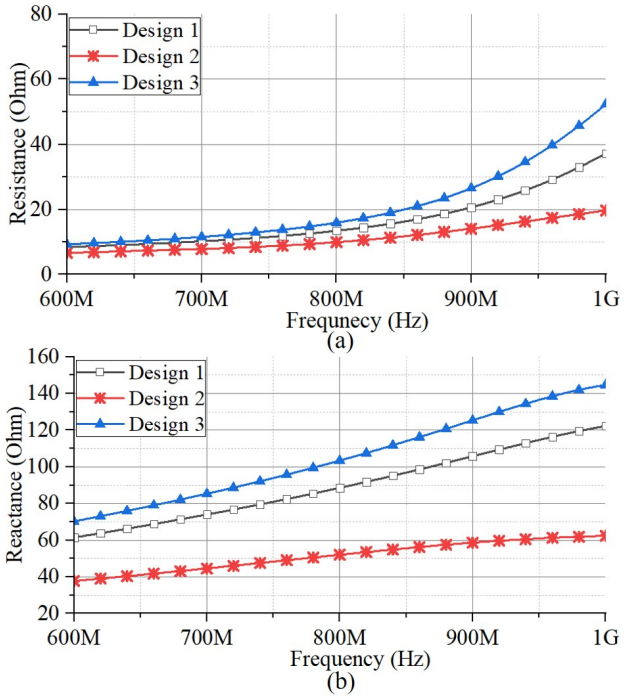

Figure 6: Simulated resistance and reactance of the three corresponding textile antennas.

the antenna patterns are embroidered by silver-plated Nylon whereas the conductive yarns have 0.2 mm thickness with corresponding bulk conductivity of 11500 siemens/m. The polyester as the substrate has relative dielectric constant, loss tangent and thickness of 1.29 (ε_r)), 0.00188 (tanD) and 0.88 mm, respectively. The simulated resistance and reactance of the three corresponding textile antennas are shown Fig. 6

Table 2: Antenna Dimension Parameters (Unit: mm)

Antenna Designs	L_1	L_2	L_3	W_1	R_1
Design 1	58	22.6	40	23.4	20
Design 2	74	15	40	22	20
Design 3	58	24.8	40	24	20

2.3.2. Antenna Manufacturing Method

To embroider the patterns on the substrate (polyester), a commercial embroidery machine (Singer Futura XL-550) is used. The embroidery procedure is detailed in Fig. 7. First of all, after obtaining appropriate designs in 3D full electromagnetic simulations, the layout models need to be exported to a type of formats which can be converted with same size into the related embroidery software. Secondly, the knit pattern size and boundaries of the designs affected slightly by embroidery modes in the embroidery software (EasyDesign EX4.0) need to be adjusted carefully. For the proposed designs, the 'satin fill' mode in the embroidery software is adopted. Finally, in the manufacturing process, the proposed yarns are utilized in both sides of the substrate as the conductive yarns and support yarns.

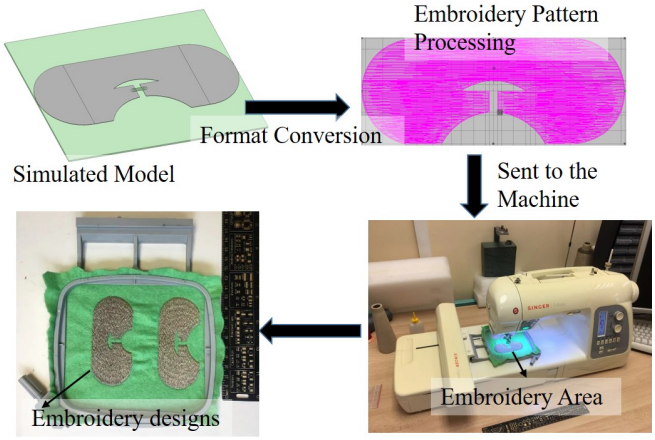

Figure 7: Embroidery procedure.

2.3.3. Impedance Simulation and Measurements of the Three Textile Antennas

As aforementioned, in order to reduce the impact from the connection, the measured complex impedance results of the case 'With Textile' are adopted as conjugate impedance of the antennas [25][26] for simulation and the simulated designs are described and shown in Fig. 5. The experimental setup is shown in Fig. 8 and the antenna impedance results are shown in Fig. 9, including the simulated and measured curves.

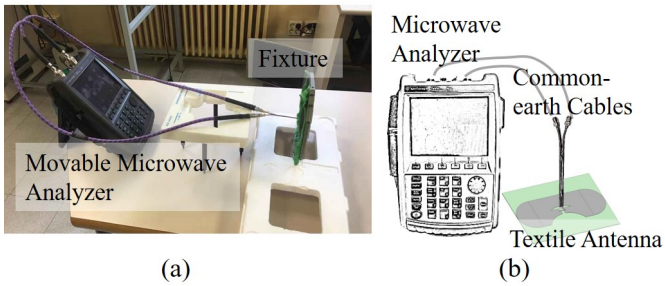

Figure 8: Experimental setup for the impedance of the embroidered designs. (a) Photograph of experimental setup, (b) Experimental setup configuration.

By analyzing the three cases, the measured impedance curves are close to the simulated curves. In addition, the simulated and measured results at 868 MHz for each case are listed in Table 3. It is found that the measured antenna impedance values are close to the conjugate impedance values of the corresponding interfaces.

Table 3: Complex Impedance of the Antenna Designs at 868 MHz(Unit: Ohm)

Case	*Design* 1	*Design* 2	*Design* 3
Simulated	17.59+i*100	12.52+i*56.77	21.93+i*117.98
Measured	28.86+i*117.8	9.24+i*60.51	23+i*115.42

2.3.4. Radiation Performance Comparison

Radiation performance is the another important factor affecting the final target of UHF-RFID tags read range. The radiation patterns in the xoy cut of the three designs are shown in Fig. 10. The maximum realized gain values of the three designs are close, 1.46 dBi, 1.38 dBi and 1.31 dBi for the design 1, design 2 and design 3, respectively.

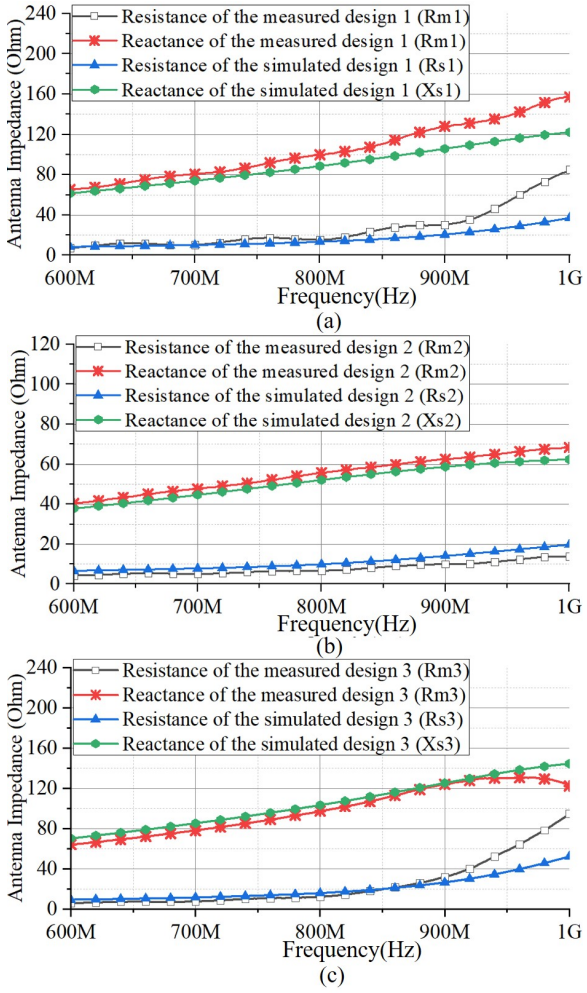

Figure 9: Simulated and measured impedance for the three corresponding textile antennas. (a) Design 1, (b) Design 2, (c) Design 3.

2.3.5. Read Range Tests

For read range tests, the experimental setup is shown in Fig. 11. In order to avoid moving the designs holders frequently, a certain distance between the read antenna and UHF-RFID tags is fixed (0.7 m) and the reader output power is adjusted. The reader antenna (MT-242025/TRH/A/A) can be controlled by the M6E Kit which is connected to a laptop with specified control software. A inquiry signal with data and clock can be adjusted by the software and sent by the reader antenna. The proposed textile UHF-RFID

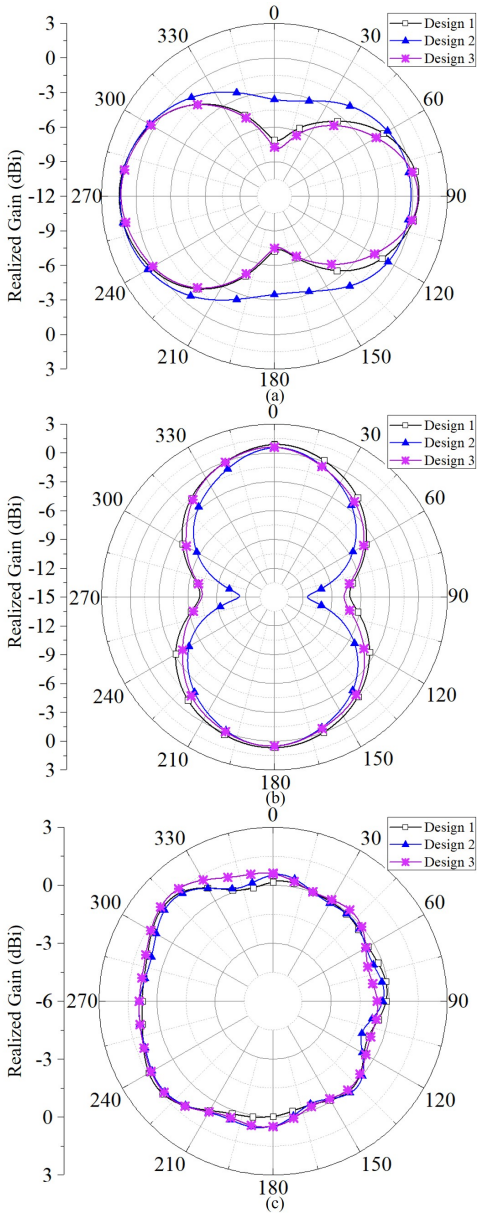

Figure 10: Simulated radiation patterns (realized gain) for the three designs.(a)XY plane, (b)XZ plane, (c)YZ plane

antennas can send a backscattered signal with data and clock after receiving the inquiry signal. The output power is adjusted until the signal transmission

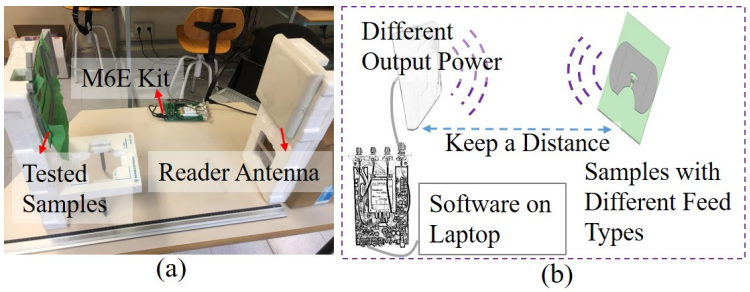

Figure 11: Experimental setup for the read ranges of the textile UHF-RFID tags. (a) Photograph of experimental setup, (b) Experimental setup configuration.

between the read antenna and the tags is disrupted. The maximum value of the read range can be calculated by the threshold power. In addition, the simulated read range can be calculated by the Friis Transmission Formula [27] as follows,

$$d_{max} = \frac{\lambda}{4\pi}\sqrt{\frac{P_t G_t G_r \cdot \tau}{P_{th}}} \tag{2}$$

where d_{max} is the maximum value of the read range, λ is the wavelength at 868 MHz, P_t is the power fed into the reader antenna, G_t is the gain of the reader antenna (7 dBi), G_r is the gain of the proposed antennas, τ is the largest power transmission coefficient (Design 1, 2 and 3: 0.6242, 0.7888 and 0.8149 at 868 MHz, respectively) and P_{th} is the minimum wake-up power of the chip(-18 dBm). In addition, the cable loss between the reader antenna and the reader is taking into account (0.8 dB).

Table 4: Simulated and Measured Maximum Read Ranges at 868 MHz in Air (Unit: m)

Case	*Type 1/Design 1*	*Type 2/Design 2*	*Type 3/Design 3*
Simulated	5.58	6.74	6.8
Measured 1st	4.52	5.19	5.82
Measured 2nd	4.57	5.25	5.69
Measured 3rd	4.47	5.25	5.76
Average Measured	4.52±0.05	5.22±0.03	5.75±0.07

For the three electro-textile interfaces with the corresponding textile antennas, the simulated and measured maximum read ranges of the type 1, 2 and 3 have been tested several times and the results are listed in Table

4. Note that the read range values are recorded when the tags can be read continuously and stably, which is not just an on-off procedure. It is found that when the realized gain and the matching situations of the three types are close, the type 3 has the better performance than the other two in simulation and measurement, respectively. The main reason for the difference between the simulated and measured results is that the real radiation and impedance cannot totally match with the simulated results due to the environmental factors, embroidery error and measuring error.

2.4. Reliability Validation

2.4.1. Mixed Use Feasibility

In the work, 'mixed use' refers to the interfaces used for other non-corresponding antennas. Generally, for each electro-textile interface, the corresponding UHF-RFID antenna is expected to be redesigned. Considering this case increases costs and design periods, the mixed use feasibility of the different electro-textile interfaces is worth exploring. Therefore, in this section the three electro-textile interfaces are applied to the three different antennas, respectively. There are nine cases, in which the test setup and related measurement method are same.

As listed in Table 5, the matched pairs have the best performance as expected. In addition, it is found that for each interface, the read ranges of the interfaces used on other two designs have tolerable decrease (< 2 m) but are all above 3.41 m. It means the unpaired combination can work normally under specific requirements. Therefore, the mixed use feasibility of the proposed electro-textile interfaces and textile UHF-RFID antennas is validated.

Table 5: Measured Read Ranges of the Nine Cases in Air (Unit: m)

Case	*Design* 1	*Design* 2	*Design* 3
Type 1	**4.5**	4.05	3.57
Type 2	3.74	**5.22**	4.29
Type 3	3.41	4	**5.75**

2.4.2. Tests On Body

In this section, the related tests on body are developed by the three connection methods (sewing by yarns, snap buttons and inserting) and the

experimental setup is shown in Fig. 12. Note that the researcher in the figure wears the winter clothes, which are thicker than normal ones and the tags can be 3 cm 4 cm from the clothes to the body with air interlayer. In the tests, all the interfaces connect to the three antenna designs, respectively, to explore the performance in the nine cases as aforementioned in last section.

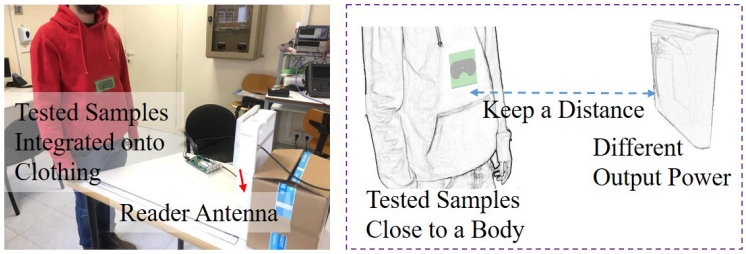

Figure 12: Experimental setup for the read ranges of the tags on body. (a) Photograph of experimental setup, (b) Experimental setup configuration.

The read range results are listed in Table 6. As expected, the read ranges for the nine cases on body are lower than that in air, respectively, due to power loss on body. However, the worst performance shows a read range of 2.05 m (the type 3 by inserting into the design 1). And all the results prove the on-body use feasibility of the interfaces with the antennas. Certainly, for attractive fashion, the electro-textile interfaces can also be hidden in thinker clothes and the textile antennas can be embroidered with other nonconductive floral patterns. When they are used on clothing, the potential as a RFID sensor such as temperature and humility sensor can be explored.

Table 6: Measured Read Ranges of the Nine Cases on Body (Unit: m)

Case	*Design* 1	*Design* 2	*Design* 3
Type 1	**3.68**	3.24	2.05
Type 2	3.43	**4.57**	3.17
Type 3	2.19	3.13	**3.35**

3. Conclusion

To conclude, three electro-textile interfaces integrated with the corresponding textile UHF-RFID antennas are proposed and evaluated in this

work. The simulated and measured impedance curves of the corresponding antennas are all close and the radiation performance (realized gain) are designed to be near (about 1.4 dBi). According to the Friis formula, the simulated and measured read ranges of the interfaces with the corresponding antennas in air are obtained (all above 4.5 m). For reliability validation, the tests for mixed use feasibility and the tests on body are implemented. The results of mixed use feasibility tests show that the read ranges of the each interface used on other two UHF-RFID antennas have tolerable decrease ($<$ 2 m) but are all above 3.41 m. It means the mixed use feasibility of the proposed electro-textile interfaces and textile UHF-RFID antennas can be proved. In addition, the read ranges of the designs on body are all above 2.05 m. Therefore, due to the small sizes of the electro-textile interfaces, stable performance on body and good reliability, the proposed electro-textile interfaces with the corresponding textile UHF-RFID antennas has potential application in the future medical and daily clothes fields.

References

[1] H. Arun, "Advancements in the use of carbon nanotubes for antenna realization," *AEU - Int. J. Electron. Commun*, vol 136, pp.153753, 2021.

[2] C. Occhiuzzi, C. Paggi and G. Marrocco, "Passive RFID Strain-Sensor Based on Meander-Line Antennas," *IEEE Trans. Antennas Propag.*, vol. 59, no. 12, pp. 4836-4840, Dec. 2011.

[3] C.Y. Luo, I. Gil, R. Fernández-García, "Wearable Textile UHF-RFID Sensors: A Systematic Review," *Materials*, vol. 13, no. 15, pp. 3292, 2020.

[4] J.C. Prather, Y. Meng, M.l Bolt, T. Horton, "Mark Adams, Wireless head impact monitoring system utilizing eye movement as a surrogate for brain movement," *AEU - Int. J. Electron. Commun*, vol. 105, pp. 54-61, 2019.

[5] Y. Shafiq, J. S. Gibson, H. Kim, C. P. Ambulo, T. H. Ware and S. V. Georgakopoulos, "A Reusable Battery-Free RFID Temperature Sensor,"*IEEE Trans. Antennas Propag.*, vol. 67, no. 10, pp. 6612-6626, Oct. 2019.

[6] Y. Wang, A. J. Pretorius and A. M. Abbosh, "Low-Profile Antenna With Elevated Toroid-Shaped Radiation for On-Road Reader of RFID-Enabled Vehicle Registration Plate," *IEEE Trans. Antennas Propag.*, vol. 64, no. 4, pp. 1520-1525, April 2016.

[7] Z. Ali, et al., "Authentication Using Metallic Inkjet-Printed Chipless RFID Tags," *IEEE Trans. Antennas Propag.*, vol. 68, no. 5, pp. 4137-4142, May 2020.

[8] C.D.M. Peña, et al., "Ultra slim and small UHF RFID tag design for mounting on curved surfaces," *AEU - Int. J. Electron. Commun*, vol 128, pp. 153502, 2021.

[9] A.H. Zarif, "A compact half butterfly chipless RFID tag based on image theory with DER analysis," *AEU - Int. J. Electron. Commun*, vol 127, pp.153486, 2020.

[10] M. Yang, et al., "A Resistance-Type Sensor Based on Chipless RFID," *IEEE Trans. Antennas Propag.*, vol. 65, no. 7, pp. 3319-3325, July 2017

[11] A. Yang, et al., "Thermal management in nanofiber-based face mask." *Nano letters*, vol 17, pp. 3506-3510, 2017.

[12] J. Wang, Q. Li, D. Liu, C. Chen, et al., "High temperature thermal conductive nanocomposite textile by "green" electrospinning," *Nanoscale*, vol. 10, pp. 16868-16872, 2018.

[13] S. Shao, A. Kiourti, R. J. Burkholder and J. L. Volakis, "Broadband Textile-Based Passive UHF RFID Tag Antenna for Elastic Material," *IEEE Antennas Wirel. Propag. Lett.*, vol. 14, pp. 1385-1388, 2015.

[14] C. Luo,1, I. Gil and R. Fernández-García, "Textile UHF-RFID antenna sensor for measurements of sucrose solutions in different levels of concentration," *Meas. Sci. Technol*, vol. 32, pp. 10, 2021.

[15] M. Tajin, C. Amanatides, G. Dion and K. Dandekar, "Passive UHF RFID-Based Knitted Wearable Compression Sensor," *IEEE Internet Things J.*, vol. 8, no. 17, pp. 13763-13773, 2021

[16] https://www.nxp.com/docs/en/data-sheet/SL3S10X4.pdf

[17] https://www.mouser.com/datasheet/2/281/UHF_RFID_Tag_LXMS21ACNP-184_datasheet_Rev1_1_18113-1877823.pdf

[18] Y. Liu, A. Levitt, C. Kara, C. Sahin, G. Dion, and K. R. Dandekar,"An improved design of wearable strain sensor based on knitted RFID technology," *2016 IEEE Conference on Antenna Measurements Applications (CAMA)*, pp. 1–4, 2016

[19] L. Shan and H. Xiao, "Impedence characterization of RFID tag antennas and application in conformal tag antenna," *2015 7th Asia-Pacific Conference on Environmental Electromagnetics (CEEM)*, Hangzhou, 2015, pp. 140-142

[20] H. Zhu, Y. C. A. Ko and T. T. Ye, "Impedance measurement for balanced UHF RFID tag antennas," 2010 IEEE Radio and Wireless Symposium (RWS), New Orleans, LA, 2010, pp. 128-131

[21] X. Qing, C. K. Goh and Z. N. Chen, "Measurement of UHF RFID tag antenna impedance," *2009 IEEE International Workshop on Antenna Technology*, Santa Monica, CA, 2009, pp. 1-4

[22] https://na.support.keysight.com/pxi/help/latest/S3_Cals/Port_Extensions.htm

[23] C.T. Carrasco, C.J. Sieiro, J.M. Lopez-Villegas, N. Vidal, R. Gonzalez-Echevarría and M.E. Roca, "Mixed-mode impedance and reflection coefficient of two-port devices," *Prog. Electromagn. Res.*, vol. 130,pp. 411-428, 2012

[24] C.K. Stoumpos, D.E. Anagnostou and M.T. Chryssomallis, "Experimental characterization of the impedance of balanced UHF RFID tag antennas," *Microw. Opt. Technol. Lett.* vol. 59(12), pp. 3127-3134, 2017

[25] M. Svanda and M. Polivka, "Matching Technique for an On-Body Low-Profile Coupled-Patches UHF RFID Tag and for Sensor Antennas," *IEEE Trans. Antennas Propag.*, vol. 63, no. 5, pp. 2295-2301, May 2015.

[26] K. Rasilainen, J. Ilvonen and V. Viikari, "Antenna Matching at Harmonic Frequencies to Complex Load Impedance," *IEEE Antennas Wirel. Propag. Lett.*, vol. 14, pp. 535-538, 2015

[27] S. Kulkarni, A. Baghel, S. Nayak, "Graded refractive index metamaterial for enhanced far-field wireless power transfer efficiency in S-band," *AEU - Int. J. Electron. Commun*, vol 138, pp.153859, 2021